RSC Advances

ROYAL SOCIETY OF CHEMISTRY

www.rsc.org/advances

Cite this: DOI: 10.1039/c0xx00000x

www.rsc.org/xxxxxx

ARTICLE TYPE

Nanoparticle-Based Hierarchical Zinc Oxide Chains for Enhanced Efficiency of Dye-Sensitized Solar Cells

Zhengdao Li,[a] Yong Zhou,[b, c *] Ruixue Sun[a], Yuhan Yang,[a] Kaijun Zhang[a]

Received (in XXX, XXX) Xth XXXXXXXXX 20XX, Accepted Xth XXXXXXXXX 20XX
DOI: 10.1039/b000000x

One-dimensional ZnO chains composed of nanoparticles were prepared using a facile method. Inspired by the unique structure as the working electrodes of the dye-sensitized solar cells (DSSCs), hierarchical ZnO chains can take both the advantages of one-dimensional (1D)-structure and nanoparticle. Superior light scattering ability, slower electron recombination rate and faster electron transport rate enhanced the photoelectric conversion performance together and show superior conversion efficiency than ZnO 1D-based DSSCs and ZnO nanoparticle-based DSSCs.

Introduction

Zinc oxide (ZnO) is considered as the most potential alternative to TiO_2 used the photoanode of dye-sensitized solar cells (DSSCs) due to its similarity to physical properties of TiO_2, higher electron mobility and ease of control over material morphologies.[1-3] In past decades, considerable effort has been devoted to increasing the conversion efficiency (η) of ZnO-based DSSCs by the synthesis of ZnO with varied architectures and morphologies attributed to increased dye loading and/or light-harvesting efficiency, the faster electron transport, and prolonged electron lifetime. [4-9]

In DSSCs, the photoelectrode film must possess a large surface area to adsorbed sufficient dye molecules in favor of capture of incident photons. The porous nanocrystalline films can satisfy this requirement and have been extensively studied.[10-13] However, this photoanode has been found to restrict the further increase of DSSC's performance due to the higher charge-recombination rate and slower electron transport.[14-16] Therefore, a variety of functional one-dimensional (1D) nanostructured ZnO photoelectrodes, such as nanotubes,[17,18] nanowires,[14,19] nanobelts[20] have been developed to tackle this issue. 1D nanostructure photoelectrodes can provide a direct transport channel for the rapid electrons transport, decreasing the possibility of charge recombination and avoiding the high resistance existing in the randomly oriented nanoparticles. However, the cell performance of simple 1D nanostructures kept at a relatively low level due to their deficient dye loading resulting from insufficient surface area.[14,21] So, the further improved η can be expected by making the photoanodes with possessed both a high surface area and fast electron transport.[22] Thus, various hierarchical ZnO structures combining multi-scale building blocks have been employed to meet these harsh requirements, including branch structure,[23] microspheres on wires,[24] tetrapod,[25] nanoflower,[26,27] and composite nanowire/nanoparticle.[28] The η of these cells were largely increased, compared to pure ZnO nanoparticle (NP) or 1D nanostructure DSSCs. However, these DSSCs either obtained η less than 4%, or were synthesized by complicated synthetic steps.

In this paper, nanoparticle-based hierarchical ZnO chains were synthesized and applied as a photoanode for DSSCs. The unique architecture has a hierarchical structure: the chain is several micrometers in length; the chain consists of interconnected ZnO nanoparticles. The chains serve as a direct pathway for fast electron transport, causing slower electron recombination rate and faster electron transport rate. Meanwhile, the nanoparticles constituted chains can provide a larger surface area than the one-dimensional ZnO rods with similar length to improve photocurrent. DSSCs fabricated from the ZnO chains gave the η of 5.06%, as a result of taking both the advantages of chains and nanoparticles.

Experimental

Preparation of the electrode

12 mmol of $Zn(CH_3COO)_2{\cdot}2H_2O$ and 36 mmol of $CO(NH_2)_2$ were added to 30 mL H_2O. The mixture was further stirred and then transferred to a 50 mL Teflon-lined stainless steel autoclave. The synthesis was performed at 120ºC for 3hrs in an electric oven. The white precipitate was filtered, washed with distilled water and dried in air naturally. Finally, the powder was calcined at different temperature and time in air for various samples. The corresponding working electrodes were fabricated according to our previous paper. [27]

ZnO rod electrodes were prepared by a precursor template method. The clean fluorine-doped tin oxide (FTO) glass was dipped in 5 mmol/ L ethanol solution of zinc acetate for 30 s, taken out, and then sintered at 350°C for 20 min. 4.5 mmol of $Zn(NO_3)_2{\cdot}6H_2O$ and 1.5 mmol of $C_6H_{12}N_4$ were added to 30 mL H_2O with continuous stirring for 10 minutes in a 50 mL stainless Teflon–lined autoclave. The FTO leaned against the inner wall of the autoclave. After the hydrothermal treatment at 100°C for 3

[a]*Chemistry and Pharmaceutical Engineering College, Nanyang Normal University, Nanyang, Henan 473061, P. R. China.*
[b]*Jiangsu Key Laboratory for Nano Technology, Eco-Materials and Renewable Energy Research Center (ERERC), Nanjing University, Nanjing, JiangSu 210093, P. R. China.*
[c]*Kunshan Innovation Institute of Nanjing University, Kunshan, Jiangsu 215300, P. R. China.*

hrs in an electric oven, the FTO was took out and washed with deionized water.

The electrodes were immersed into N719 ethanol solution for 90 mins. A magnetron sputter Pt mirror served as the counter electrode. The FTO substrate, film, and counter electrode constituted a sandwich-like open cell. A drop of the electrolyte was injected into the cell, which composed of 30 mM I_2, 0.5 M *tert*-butylpyridine, 1.0 M 1-Butyl-3-methylimidazolium iodide (BMIMI) and 50 mM LiI, in a mixed solvent of valeronitrile and acetonitrile (v/v, 15:85).

Characterization

The morphology was characterized using the transmission electron microscopy (TEM, JEOL 3010, Japan) and scanning electron microscopy (SEM, FEI NOVA NanoSEM230, USA). Thermogravimetric (TG) analysis was performed on an American TA SDT Q600 analyzer in the temperature from 25°C to 700°C. The X-ray diffraction (XRD) data were measured by X-ray diffractometer with Cu-K□□radiation at 40 kV and 200 mA. To quantify the amount of adsorbed the dye, N719 was desorbed into a 0.1 M NaOH aqueous solution, and the optical absorption spectra of the solution were collected using a UV-vis spectrophotometer. Shimadzu UV-2550 UV-vis spectrometer was used to investigate the diffuse reflectance spectrum and optical absorption of powder. The incident-photon-to-current conversion efficiency (IPCE) spectra were recorded on PEC-S20 (Peccell Technology). The photocurrent–voltage characteristics (*J-V*) were performed under a sunlight simulator with an active area of 0.132 cm^2 (Oriel 92251A-1000, AM 1.5 globe, 100 mW cm^{-2}). Intensity-modulated photovoltage/photocurrent spectra (IMVS/IMPS) were performed using the electrochemical workstation (Zahner, Zennium).

Results and discussion

The SEM image of the precursor shows that its morphology is sheet with smooth surfaces (see ESI,† Fig. S1a). The XRD peaks of the precursor presented in Fig. S2a (ESI†) are attributed to hydrozincite $Zn_5(OH)_6(CO_3)_2$ (JCPDS #72-1100). ZnO samples with different morphologies generate after annealing precursor under different treating temperature and time. When the precursor was calcined at 450 °C for 30 minutes, porous ZnO nanosheets were fabricated. The sheet morphology is maintained, but numerous nanopores are formed in the sheet as shown in Fig. S1b. This could be ascribed to the release of H_2O and CO_2 during the heat treatment of $Zn_5(OH)_6(CO_3)_2$ (see ESI,† Fig. S3). When the calcination temperature increases to 500°C, as-synthesized powder display the chain feature with a diameter of 150~200 nm and length of 10~15 μm in Fig. 1a (labeled as P1). The enlarged SEM image reveals the building blocks for the chain are particle structures with a diameter of 50~70 nm (Fig. 1b). It is noteworthy that thicker chains with sub-micrometer diameter are composed of simple chains and marked by an arrow in Fig. 1c, which could generate an efficient scattering center to enhance the light-harvesting capability. The TEM images in Fig. 2a and b further show the single ZnO chain and thicker sub-micrometer chains are constructed of interconnected nanoparticles with a diameter of 50~70 nm. Fig. 2c is the HRTEM image taken from the between of two nanoparticles. A lattice spacing of 0.26 nm could be attributed to the (101) plane of the hexagonal ZnO. For comparison, the ZnO nanoparticles with the diameter of 50~70 nm were observed after calcination in air at 550°C for 3 hrs (labeled as P2, see ESI,† Fig. S1c and d). Fig. S1f (ESI†) is a cross-sectional SEM of the synthesized ZnO rods photoanodes (labeled as P3), showing vertically oriented ZnO arrays grown on the substrate with 12 μm in average length and 500~600 nm in diameter. The XRD patterns of all samples correspond well to the hexagonal ZnO (a = b = 0.3249nm, c =0.5205nm, α = β =90°, γ =120°, JCPDS Card File No. 89-0511) (see ESI,† Fig. S2b).

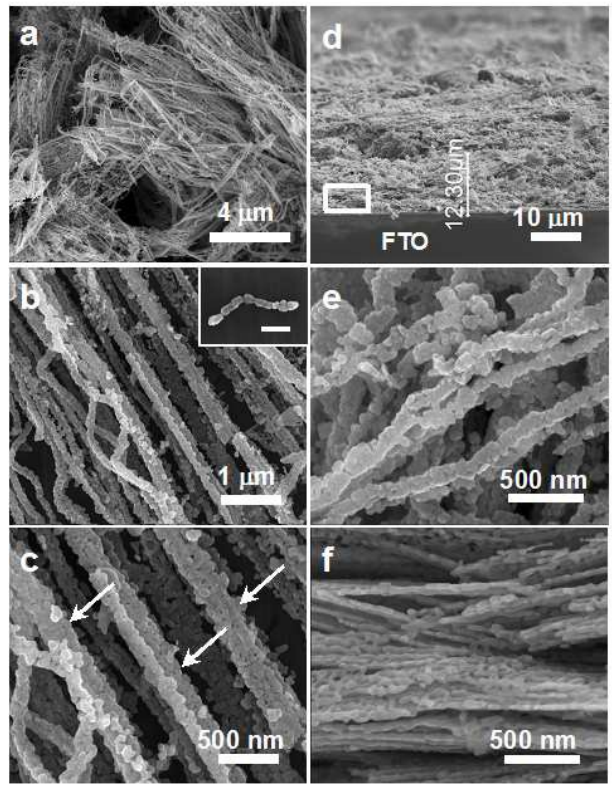

Fig. 1. SEM images of: (a-c) the ZnO chains at different magnification. (d) cross section of the ZnO chains photoanode. (e) top view of the ZnO chains photoanode. (f) high magnification view from the squared region of part d. Inset: the scale bars is 200 nm in (b).

Fig. 3 compares the effect of ZnO morphologies on performance and their corresponding characteristics, open-circuit voltages (V_{oc}), fill factors (FF), short-circuit current (J_{sc}) and η, are tabulated in the inset table. The DSSCs assembled with ZnO chains exhibit η of 5.06% with J_{sc} of 14.53 mA/cm^2, V_{oc} of 0.57V, and a FF of 60.92%, which is higher than η of ZnO nanoparticle (P2, 3.62%) and ZnO rod (P3, 2.78%). The remarkable improved η is the results from the larger J_{sc}, compared with that obtained from the P2 (10.97 mA/cm^2) and P3 (8.27 mA/cm^2). In the given ZnO/dye/electrolyte system, the variation in the J_{sc} could be attributed to the dye adsorption amount or/and light-harvesting efficiency.[29] The surface areas of P1, P2 and P3 is 18.26 m^2 g^{-1}, 27.29 m^2 g^{-1} and 7.32 m^2 g^{-1}, then, the corresponding amount of dye adsorption is 4.6×10^{-8} mol/cm^2, 6.2×10^{-8} mol/cm^2 and 2.2×10^{-8} mol/cm^2, respectively. The nanoparticles constituted

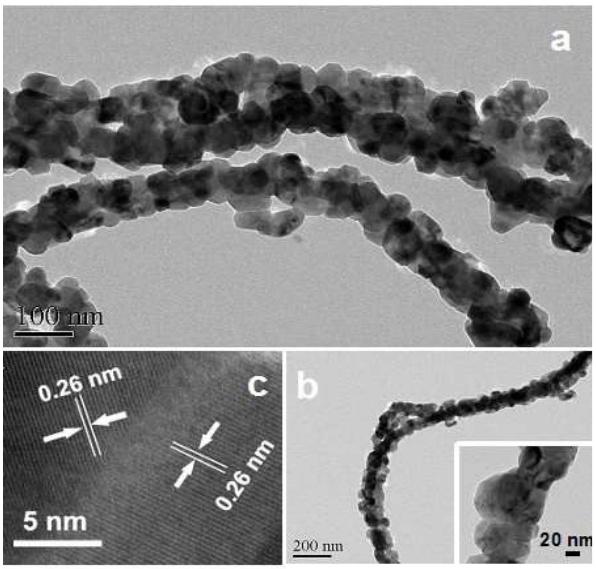

Fig. 2. (a, b) TEM and (c) HRTEM image of the ZnO chains.

chains can provide chains with a larger surface area than the ZnO rods with similar length, which are responsible for the improved photocurrent. Since the dye absorption amount on the P1 is less than that of the P2, the enhanced J_{sc} value for the P1 should be due to the light-harvesting efficiency. To analyze more detail in the light-harvesting efficiency, the diffuse-reflection spectrum was conducted (Fig. 4a). It is apparent that the intensity increases in the order of P3, P2 and P1 at wavelengths from 450 to 800 nm, which can be explained due to the different structure. Firstly, it is believed that resonant scattering can occur when the medium size is comparable to the wavelength of incident light.[30] Herein, the thicker chains with sub-micrometer diameter in P1 films could act as an efficient scattering center to improve light-harvesting efficiency.[31] Secondly, prior studies have demonstrated that admixing large particles into nanocrystalline films could enhance the light-harvesting capability of photoelectrodes.[32,33] The P1 films assembled by staggered thick and thin chains can achieve the same effect (Fig. 1e).[34] Thirdly, the high magnification cross-sectional view of a 12μm-thick chain film photoanodes indicates a multilayer morphology aligned horizontally (Fig. 1f). The incident light goes through the photoanode layer by layer and, at the same time, scatters in them, which increases the optical path length inside DSSCs and the opportunities for light absorption; Furthermore, to confirm our conclusions, IPCE spectra were collected (Fig. 4b). The increased IPCE value at 370–600 nm wavelengths could be attributed to higher dye loading amount. At the long wavelength (600–750 nm), the higher IPCE values could be ascribed to the improved scattering effect of the film.[35] The IPCE of ZnO chains-based films is higher at 550–750 nm than that of nanoparticles, suggesting the J_{sc} increment of ZnO chains-based films is attributed to the improved light scattering effect.

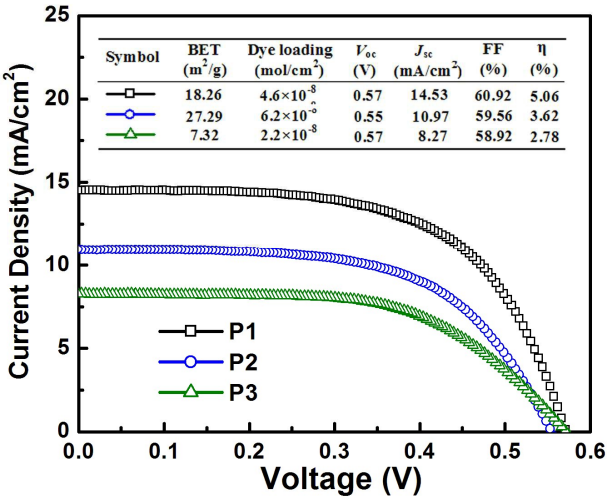

Fig. 3. *J–V* curves for cells based on different ZnO electrodes. Photoanode thickness: 12 μm.

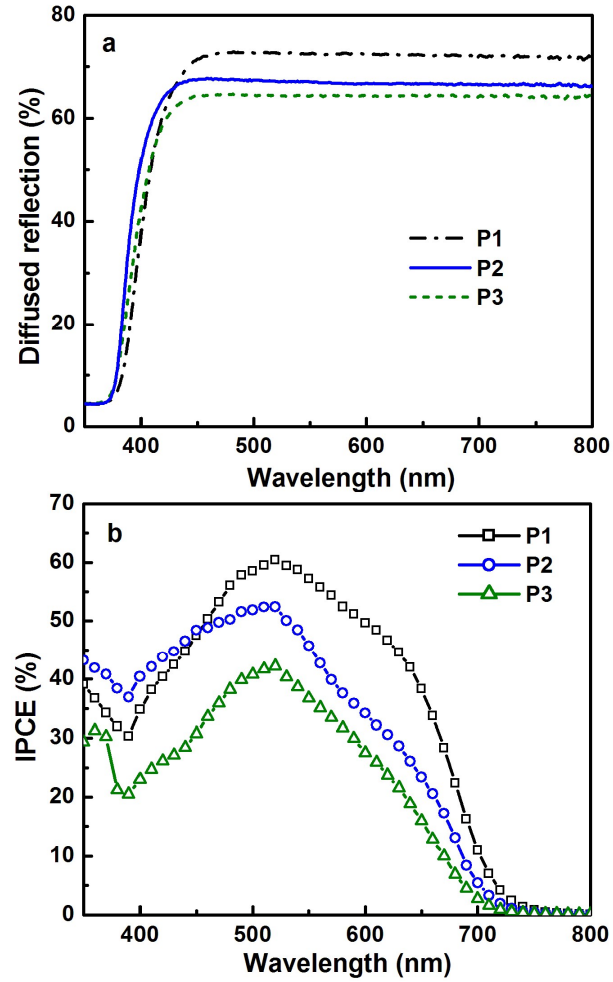

Fig. 4. (a) Diffuse reflectance spectra and (b) IPCE curves of the different ZnO electrodes.

To investigate electron transfer properties and charge recombination reaction, IMPS/IMVS measurements were carried out under irradiation intensity from 30 to 150 W/m^2 (Fig. 5). The electron transport time (electron lifetime) can be estimated from the equations $\tau_d=1/2\pi f_d$ ($\tau_r=1/2\pi f_r$), where f_d (f_r) is the characteristic frequency at the minimum of IMPS (IMVS)

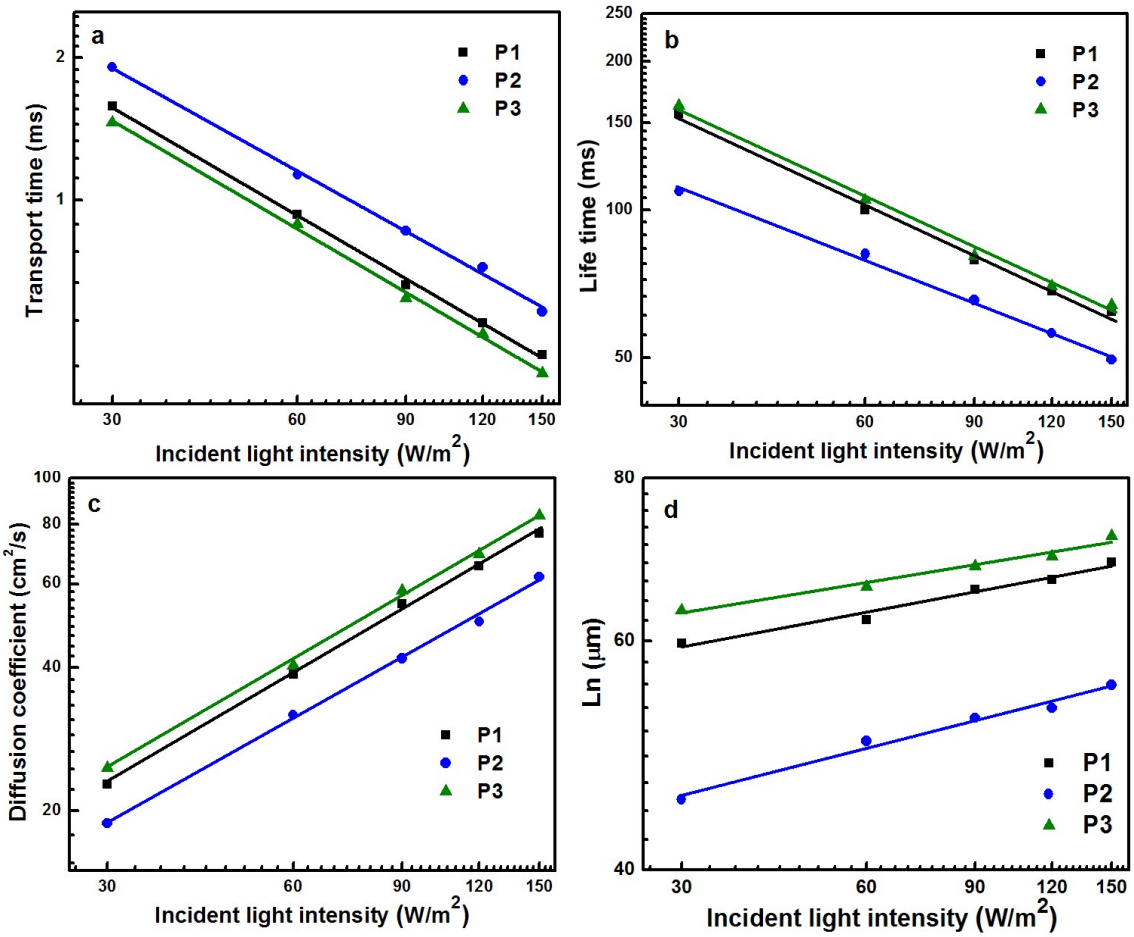

Fig. 5. (a) Transport time (b) Lifetime (c) electron diffusion coefficients and (d) the effective electron diffusion length based on the different photoelectrodes.

imaginary component (Fig. 5a and b).[36] Obviously, the τ_d of P1-based DSSCs is similar to the value of the P3-based DSSCs and considerably shorter than that of the P2-based DSSCs under diverse light intensity, implying the faster transport rate than that of P2. This result verified that the ZnO chains are in favour of the electron transport compared to ZnO nanoparticles of random transfer pathway. The τ_r based on P1 photoanode is longer than that of P2, indicating the longer electron lifetime and is responsible for the higher V_{oc} of the former.[37] This result is attributed to fewer nanocrystalline boundaries and electron trapping sites for ZnO chains compared with the ZnO nanoparticles.[14] It is generally known that the surface charge trap-site density could have a great impact on the charge recombination. The more trap sites would cause the faster charge recombination. Compared with P2, the P1 has relatively fewer grain boundaries and crystal defects, which results in the smaller trap site density, so reduced charge recombination can be expected [38]. Furthermore, electron diffusion coefficient (D_n= $d^2/(4\tau_d)$, d: film thickness) is highest in P3 and lowest in P2 (Fig. 5c). The higher the value of D_n, the faster the transmission speed of the photogenerated electrons to the anode contact [39]. Electrons in the ZnO chains structure are slightly lower than ZnO rods but faster than ZnO nanoparticles. This is because the ZnO rods and chains photoanodes can provide direct transport pathway for rapid collection of electrons.[32,39] In contrast, ZnO nanoparticles would offer more traps in the nanocrystalline boundaries, in which the electron could be trapped during the transmission to some extent.[14] The effective electron diffusion length (L_n=$(D_n\tau_r)^{1/2}$) of P1 is longer than that of P2 at different light intensity, which suggest that the chain-based DSSCs is obviously superior to naoparticle-based DSSCs for a given recombination loss, associated with high η.[40] Although the ZnO rod-based DSSCs demonstrates the superior electron transport velocity to ZnO chains-based DSSC, insufficient amount of dye loading limits the generation of J_{sc}, leading to a relatively lower η; Despite having larger surface areas than ZnO chains-based device, ZnO nanoparticle-based device show lower efficiencies, which ascribe to inferior light scattering capacity for boosting the light-harvesting efficiency to those ZnO chains. Having considered all the factors above, the significant improvement of η for the nanoparticle-based hierarchical ZnO chains can be ascribed to its taking both the advantages of chains and nanoparticle. Superior light scattering ability, slower electron recombination rate, faster electron transport rate are responsible for the enhanced η.

Conclusions

In summary, hierarchical ZnO chains composed of nanoparticles were prepared as photoanodes for DSSCs by a facile method. The experimental researches showed that ZnO samples with different morphologies derive from different treating temperature and time. ZnO chains with maximum energy conversion efficiency were formed at 500 °C for 0.5 h by annealing precursor. The investigations revealed that the nanoparticles constituted chains can provide chains with a larger surface area than the 1D ZnO rods with similar length, which were responsible for the improved photocurrent. Meanwhile, the chains can provide the direct electrical pathways for the collection of photogenerated electrons and present slower electron recombination rate and faster electron transport rate than nanoparticles due to the presence of far fewer surface defects and grain boundaries than the latter. The DSSCs fabricated from such hierarchical structure gived a conversion efficiency of 5.06%, far higher than 2.78% of ZnO rod-based DSSCs, and 3.62% of ZnO nanoparticle-based DSSCs, as a result of taking both the advantages of chains and nanoparticles.

Notes and references

This work was supported by 973 Programs (No. 2011CB933303, 2014CB239302, 2013CB632404), NSFC (No. 21301101 and 11174129), Natural Science Foundation of Jiangsu Province (No. BK2012015 and BK2011056), Jiangsu Technical support plan-industrial parts (BE2012089), Kunshan New industries multiplication plan science and technology special Fund (KX1202), Natural Science Foundation of Nanyang Normal University (No. ZX2014040 and QN2015010).

Notes and references

1 Q. Zhang, C. S. Dandeneau, X. Zhou and G. Cao, *Adv. Mater*., 2009, **21**, 4087.
2 H. Pan, N. Misra, S. H. Ko, C. P. Grigoropoulos, N. Miller, E. E. Haller and O. Dubon, *Appl. Phys. A*, 2009, **94**, 111.
3 J.A. Anta, E. Guillén and R. Tena-Zaera, *J. Phys. Chem. C*, 2012, **116**, 11413.
4 Q. Zhang and G. Cao, *J. Mater. Chem*., 2011, **21**, 6769.
5 Z. Dong, X. Lai, J. E. Halpert, N. Yang, L. Yi, J. Zhai, D. Wang, Z. Tang and L. Jiang, *Adv. Mater*., 2012, **24**, 1046.
6 Q. Zhang, T. Chou, B. Russo, S. A. Jenekhe and G. Cao, *Adv. Funct. Mater*., 2008, **18**, 1654.
7 H. Dong, L. Wang, R. Gao, B. Ma and Y. Qiu, *J. Mater. Chem*., 2011, **21**, 19389.
8 C. Wu and J. Wu, *J. Mater. Chem*., 2011, **21**, 13605.
9 Y. Lai, C. Lin, H. Chen, J. Chen, C. Kung, R. Vittal and K. C. Ho, *J. Mater. Chem*., 2010, **20**, 9379.
10 S. B. Ambade, R. S. Mane, S.-H. Han, S.-H. Lee, M.-M. Sung and O.-S. Joo, *J. Photochem. Photobiol. A*, 2011, **222**, 366.
11 G. Pérez-Hernández, A. Vega-Poot, I. Pérez-Juárez, J. M. Camacho, O. Arés, V. Rejón, J. L. Peña and G. Oskam, *Sol. Energy Mater. Sol. Cells*, 2012, **100**, 21.
12 K. Keis, E. Magnusson, H. Lindstrom, S. E. Lindquist and A. Hagfeldt, *Sol. Energy Mater. Sol. Cells*, 2002, **73**, 51.
13 T. Yoshida, J. B. Zhang, D. Komatsu, S. Sawatani, H. Minoura,T. Pauporte, D. Lincot, T. Oekermann, D. Schlettwein, H. Tada, D. Wohrle, K. Funabiki, M. Matsui, H. Miura and H. Yanagi, *Adv. Funct. Mater*., 2009, **19**, 17.
14 M. Law, L. E. Greene, J. C. Johnson, R. Saykally and P. D. Yang, *Nat. Mater*., 2005, **4**, 455.
15 K. Zhu, N. R. Neale, A. Miedaner and A. J. Frank, *Nano Lett*., 2007, **7**, 69.
16 D. Chen, H. Zhang, S. Hu and J. H. Li, *J. Phys. Chem. C*, 2008, **112**, 117.
17 M. Guo, P. Diao and S. M. Cai, *Chem. Lett*., 2004, **15**, 1113.
18 A. B. F. Martinson, J. W. Elam, J. T. Hupp and M. J. Pellin, *Nano Lett*., 2007, **7**, 2183.
19 G. Chen, K. Zheng, X. Mo, D. Sun, Q. Meng and G. Chen, *Mater. Lett*., 2010, **64**, 1336.
20 X. D. Wang, Y. Ding, C. J. Summers and Z. L. Wang, *J. Phys. Chem. B*, 2004, **108**, 8773
21 J. B. Baxter and E. S. Aydil, *Appl. Phys. Lett*., 2005, **86**, 053114.
22 B. O'Regan and M. Grätzel, *Nature*, 1991, **353**,737.
23 S. H. Ko, D. Lee, H. W. Kang, K. H. Nam, J. Y. Yeo, S. J. Hong, C. P. Grigoropoulos and H. J. Sung, *Nano Lett*., 2011, **11**, 666.
24 X. Kang, C Jia, Z. Wan, J. Zhuang and J, Feng, *RSC Adv*., 2015, **5**, 16678.
25 W. Chiu, C.H. Lee, H. Cheng, H. Lin, S.C. Liao, J.M. Wu, W.F. Hsieh, *Energy Environ. Sci*., 2009, **2**, 694.
26 İ. Şişman, M. Can, B. Ergezen and M. Biçer, *RSC Adv*., 2015, **5**, 73692.
27 Z. Li, Y. Zhou, J. Zhang, W. Tu, Q. Liu, T. Yu, Z. Zou, *Crystal Growth & Design*, 2012, **12**, 1476.
28 S. Yodyingyong, Q. Zhang, K. Park, C.S. Dandeneau, X. Zhou, D. Triampo and G. Cao, *Appl. Phys. Lett*., 2010, **96**, 073115.
29 J. Qian, P. Liu, Y. Xiao, Y. Jiang, Y. Cao, X. Ai, H. Yang, *Adv. Mater*., 2009, **21**, 3663.
30 P. E. Wolf, G. Maret, *Phys. Rev. Lett*., 1985, **55**, 2696.
31 S. Hore, P. Nitz, C. Vetter, C. Prahl, M. Niggemann, R. Kern, *Chem. Commun*., 2005, 2011.
32 Q. Zhang, T. P. Chou, B. Russo, S. A. Jenekhe and G. Cao, *Angew. Chem*., 2008, **120**, 2436.
33 S. Nishimura, N. Abrams, B. A. Lewis, L. I. Halaoui, T. E. Mallouk, K. D. Benkstein, J. van de Lagemaat and A. J. Frank, *J. Am. Chem. Soc*., 2003, **125**, 6306.
34 Y. Rui, Y. Li, H. Wang and Q. Zhang, *Chem. Asian J*., 2012, **7**, 2313.
35 M. Grätzel, *Inorg. Chem*., 2005, **44**, 6841.
36 H. X. Wang, P. G. Nicholson, L. Peter, S. M. Zakeeruddin and M. Grätzel, *J. Phys. Chem. C*, 2010, **114**, 14300.
37 Y. Wang, W, Zhao, X. Li and D. Li, *Electrochim. Acta*, 2015, **151**, 399.
38 I. Shiyanovskaya and M. Hepel, *J. Electrochem. Soc*., 1999, **146**, 243.
39 Y. Cui, L. Zhang, K. Lv, G. Zhou and Z. Wang, *J. Mater. Chem. A*, 2015, **3**, 4477.
40 M. Kim, K.-W. Lee, L. Jang, D. Jeon, J. Ju, H. Yun and I. Lee, *Electrochim. Acta*, 2014, **133**, 610.

Cite this: DOI: 10.1039/c0xx00000x

www.rsc.org/xxxxxx

ARTICLE TYPE

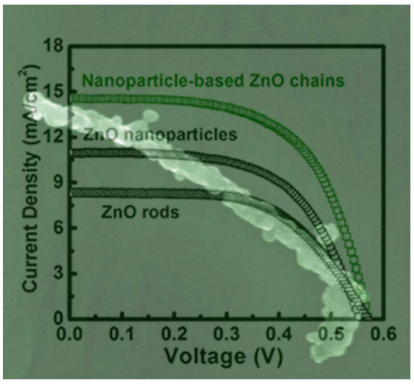

One-dimensional ZnO chains composed of nanoparticles were prepared as the working electrodes of the DSSCs, which can take both the advantages of 1D-structure and nanoparticle, show superior photoelectric conversion performance.